Rolling-Horizon Electric Vertical Takeoff and Landing Arrival Scheduling for On-Demand Urban Air Mobility

滚动时间窗口电动垂直起降到达调度策略研究: 面向按需城市空中出行

Imke C. Kleinbekman* and Mihaela Mitici ‡
Imke C. Kleinbekman* 和 Mihaela Mitici ‡
Delft University of Technology, 2926 HS Delft, The Netherlands
代尔夫特理工大学，2926 HS 代尔夫特，荷兰
and
以及
Peng Weiß
彭伟
Iowa State University, Ames, Iowa 50011
爱荷华州立大学，艾姆斯，爱荷华州 50011https://doi.org/10.2514/1.I010776

Urban air mobility with electric vertical takeoff and landing (eVTOL) vehicles is envisioned to become a fast and flexible urban transportation mode. Apart from technical challenges for eVTOLs regarding vehicle design and manufacturing, airspace design and traffic control mechanisms are most desired on the operation side. In particular, from an operational point of view, the arrival phase is expected to be the main bottleneck, with restricted vertiport resources, high air traffic density, frequent flight maneuvers, and limited eVTOL remaining battery energy, all leading to complex operational constraints. This work provides a framework to enable optimal and efficient on-demand eVTOLs arrivals in the context of on-demand urban air mobility. This paper investigates the throughput of a double-landing-pad vertiport by proposing a new vertiport terminal area airspace design and a novel rolling-horizon scheduling algorithm with route selection capability to compute the optimal required time of arrival for eVTOLs in a tactical manner. Finally, a case study on arrivals in a hexagonal vertiport network is performed to show the algorithm performance with different configurations. Our simulation results show that up to 50 s delay per eVTOL is expected during the commuter peak hours and less than 10 s delay is expected during off-peak hours.

城市空中出行，采用电动垂直起降 (eVTOL) 车辆，被设想成为一种快速、灵活的城市交通模式。除了关于 eVTOL 车辆设计制造的技术挑战之外，在运营方面，对空域设计和交通控制机制的需求最为迫切。特别是从运营的角度来看，到达阶段预计将是主要的瓶颈，受限于垂直机场资源、高空中交通密度、频繁的飞行机动以及有限的 eVTOL 剩余电池能量，所有这些因素都导致了复杂的运营约束。本文提供了一个框架，以实现按需城市空中出行背景下 eVTOLs 的最优和高效到达。本文通过提出一种新的垂直机场终端区域空域设计和一个创新的滚动时间窗口调度算法，该算法具有航线选择能力，以战术方式计算 eVTOLs 所需的最优到达时间。最后，对一个六边形垂直机场网络中的到达进行了案例研究，以展示算法在不同配置下的性能。我们的仿真结果显示，在通勤高峰时段，每架 eVTOL 预计将出现最多 50 s 的延误，而在非高峰时段，预计的延误将少于 10 s 。

I. Introduction

I. 引言

URBAN air mobility (UAM) with electric vertical takeoff and landing (eVTOL) vehicles is envisioned to become a customized, on-demand air transportation mode, by carrying passengers and cargo safely and efficiently within urban areas. As cities and streets become more congested, UAM offers the potential for significant commute time savings compared with ground transportation modes.

城市空中出行 (UAM) 利用电动垂直起降 (eVTOL) 车辆，预计将成为一种定制化的、按需的空中交通模式，它可以在城市区域内安全高效地运送乘客和货物。随着城市和街道变得越来越拥堵，UAM 与地面交通方式相比，具有显著减少通勤时间的潜力。

Companies such as Airbus, Bell, Embraer, Joby Aviation, Kitty Hawk, Pipistrel, Volocopter, and Aurora Flight Sciences have been designing, building, and testing innovative eVTOL aircraft for UAM operations [1]. The UAM industry is facing several challenges regarding vehicle design and manufacturing, such as battery technology, assured vehicle autonomy, and scalable manufacturing process. Moreover, in order to make UAM a reliable and practical transportation mode, operational challenges must be addressed. In particular, there is a need for airspace design and air traffic control mechanisms to enable safe and efficient UAM operations with these eVTOL aircraft. In this paper, we focus on solving one

particular phase of the UAM operations, that is, UAM arrivals at a vertiport, by leveraging airspace design/configuration, trajectory optimization, eVTOL battery modeling, and arrival scheduling to support safe and efficient flight operations for on-demand, UAM arrivals.

如空中客车、贝尔、巴西航空工业公司、Joby Aviation、Kitty Hawk、Pipistrel、Volocopter 和 Aurora Flight Sciences 等公司一直在设计、制造和测试用于 UAM 运营的创新型 eVTOL 飞机 [1]。UAM 行业在车辆设计和制造方面面临多项挑战，例如电池技术、确保车辆自主性以及可扩展的制造流程。此外，为了使 UAM 成为一种可靠且实用的交通方式，必须解决运营方面的挑战。特别是，需要设计空域和空中交通控制机制，以实现这些 eVTOL 飞机的安全高效 UAM 运营。在本文中，我们专注于解决 UAM 运营的一个特定阶段，即 UAM 在垂直机场的到达，通过利用空域设计/配置、轨迹优化、eVTOL 电池建模和到达调度，以支持按需 UAM 到达的安全高效飞行运营。

In contrast to the small drones that can take off and land almost anywhere covered by UTM services, eVTOL vehicles in UAM operations need to take off from and land at specific ground infrastructures called vertiports. A vertiport is an airport for VTOL vehicles. It could range from a single landing pad on top of a parking structure to a larger building with multistory landing pads that could redefine the urban architecture and city planning [2]. When UAM traffic grows, one of the major emerging bottlenecks is expected to be the limited number of vertiports and landing pads. As such, UAM arrivals will become the most safety-critical flight phase due to limited resource of vertiport landing pads, high-density traffic in terminal airspace, frequent flight maneuvers, and low remaining battery energy for eVTOLs. Therefore, in this paper we propose a suite of mechanisms for tactical UAM arrival management, among which the rolling-horizon arrival scheduling algorithm enables a double-landing-pad vertiport to land peak-hour eVTOLs with less than 50 s average delay per aircraft.

与几乎可以在 UTM 服务覆盖的任何地方起飞和降落的小型无人机相比，UAM 运营中的 eVTOL 车辆需要从特定的地面基础设施——称为垂直机场的场所起飞和降落。垂直机场是 VTOL 车辆的机场。它可能从一个停车结构顶部的单个着陆垫到一个多层着陆垫的大型建筑，后者可以重新定义城市建筑和城市规划 [2]。当 UAM 交通增长时，预计出现的其中一个主要瓶颈将是垂直机场和着陆垫的数量有限。因此，由于垂直机场着陆垫资源有限、终端空域高密度交通、频繁的飞行机动以及 eVTOL 剩余电量低，UAM 抵达将成为最关键的安全飞行阶段。因此，在本文中，我们提出了一套用于战术 UAM 抵达管理的机制，其中包括滚动时间窗口抵达调度算法，该算法能够使双着陆垫的垂直机场在高峰时段降落的 eVTOL 的平均延迟每架飞机少于 50 s 。

The contribution of this paper is twofold. First, we propose a vertiport terminal area airspace design 13 with a double-landing-pad vertiport and multiple arrival routes. Second, based on this airspace structure, we develop a rolling-horizon optimization algorithm that sequences and schedules multiple eVTOLs arriving at the vertiport. Our algorithm extends existing arrival optimization models designed for commercial aviation [3 – 5] . The eVTOLs we consider are constrained by their remaining battery energy and their flight performance parameters. Our aim is to minimize the total eVTOL arrival delay at the vertiport. We formulate this problem as a rolling-horizon, mixed-integer linear program. We determine an optimal required time of arrival (RTA) for eVTOLs arriving at the vertiport. These RTAs are the decision variables in our optimization model, that is, the required time for the eVTOLs to arrive at the vertiport. Finally, we apply our sequencing and scheduling optimization algorithm in a case study on arrivals at a hexagonal vertiport network in Houston, TX. The performance of our algorithm is evaluated for different vertiport configurations. Our simulation results show that, during peak hours, at least two landing pads are needed to accommodate the demand. Moreover, we also show that during the peak hours, up to 50 s delay per eVTOL is expected, whereas during off-peak hours, less than 10 s delay per eVTOL is expected.

本文的贡献有两方面。首先，我们提出了一种带有双降落垫的直升机场终端区域空域设计方案，并设有多个到达路线。其次，基于这种空域结构，我们开发了一种滚动时间视野优化算法，用于对抵达直升机场的多个 eVTOL 进行排序和调度。我们的算法扩展了现有针对商业航空设计的到达优化模型 [3 – 5] 。我们所考虑的 eVTOL 受到剩余电池能量和飞行性能参数的限制。我们的目标是最小化直升机场 eVTOL 的总到达延误。我们将此问题构建为一个滚动时间视野的混合整数线性规划问题。我们确定了抵达直升机场的 eVTOL 所需的最优到达时间 (RTA)。这些 RTA 是我们优化模型中的决策变量，即 eVTOL 到达直升机场所需的时间。最后，我们在德克萨斯州休斯敦的一个六边形直升机场网络到达案例研究中应用了我们的排序和调度优化算法。我们评估了算法在不同直升机场配置下的性能。我们的模拟结果显示，在高峰时段，至少需要两个降落垫来满足需求。此外，我们还表明，在高峰时段，预计每个 eVTOL 的延误可达 50 s ，而在非高峰时段，每个 eVTOL 的延误预计少于 10 s 。

The remainder of this paper is organized as follows. In Sec. II we discuss existing literature on eVTOL operations. In Sec. III we present a model for eVTOLs arrival sequencing and scheduling at a double-landing-pad vertiport. In Sec. IV we present sequencing and scheduling results for an EHANG 184 arriving at a double-landing-pad vertiport. In Sec. VI we provide conclusions and recommendations

for future work.

本文的其余部分组织如下。在第二节中，我们讨论了关于 eVTOL 运营的现有文献。在第三节中，我们提出了一个用于双降落垫直升机机场的 eVTOL 到达序列和调度模型。在第四节中，我们展示了 EHANG 184 到达双降落垫直升机机场的序列和调度结果。在第六节中，我们提供了结论以及对未来工作的建议。

II. Related Work

II. 相关工作

Current UAM research efforts are mainly focused on the design of an urban airspace for UAM [2, 6, 7] , on UAM demand forecasting [7, 8] , and on the design of the vehicles.

当前城市空中出行 (UAM) 的研究工作主要集中在为 UAM 设计城市空域 [2, 6, 7] ，UAM 需求预测 [7, 8] ，以及车辆的设计上。

One of the most pressing operational challenges for near-terminal on-demand UAM operations is the sequencing and scheduling of arrivals because eVTOL flight time is constraint by the remaining life of their electric batteries, the capacity of vertiports is limited, and the operations do not follow a predefined arrival schedule. For commercial aviation, where the terminal area exhibits complex arrival trajectories [9], a significant amount of research has addressed the problem of aircraft arrival sequencing and scheduling at an airport [3 − 5, 10, 11] . However, none of these models consider the remaining flight time as a constraint, as is the case in this paper, where the eVTOL arrivals scheduling problem is restricted by the flight time supported by electric batteries. In fact, research focused on commercial aviation aims at optimizing the arrival process by minimizing the fuel consumption [12] or by optimally sequencing the arrival to avoid fuel shortage [13], whereas the electric battery flights supported by eVTOLs pose new battery-related constraints. Various aspects of eVTOL arrival procedures have been investigated in [14, 15] . In [14] an eVTOL vehicle routing, departure, and arrival scheduling is developed such that minimum separation is ensured. Here, eVTOL traffic is integrated with existing air traffic. In our previous work [15] we propose an arrival sequencing and scheduling algorithm that minimizes eVTOL delay while considering limited battery power and limited, one-landing-pad vertiport capacity.

近终端按需城市空中交通 (UAM) 运营面临的最紧迫的运营挑战之一是 Arrival 的排序和调度，因为 eVTOL 的飞行时间受到其剩余电量的限制，垂直机场的容量有限，且运营不遵循预定的到达时间表。对于商业航空，终端区域呈现出复杂的到达轨迹 [9]，已有大量研究解决了机场飞机到达排序和调度问题 [3 − 5, 10, 11] 。然而，这些模型均未考虑剩余飞行时间作为约束，这在本文中有所不同，本文中 eVTOL 到达调度问题受到电动电池支持的飞行时间的限制。实际上，专注于商业航空的研究旨在通过最小化燃油消耗 [12] 或通过优化到达顺序以避免燃油不足 [13] 来优化到达过程，而 eVTOL 支持的电动电池飞行带来了新的电池相关约束。文献 [14, 15] 中研究了 eVTOL 到达程序的各个方面。在 [14] 中，开发了一种 eVTOL 车辆的路线、出发和到达调度方法，以确保最小间隔。在这里，eVTOL 交通与现有空中交通相结合。在我们之前的工作 [15] 中，我们提出了一种到达排序和调度算法，该算法在考虑有限的电池电量和有限的、单着陆垫的垂直机场容量时，最小化 eVTOL 延迟。

Existing literature regarding electric battery discharge models for aircraft is limited. In [16-18] battery modeling and predictions for electric winged aircraft are proposed based on flight testing. In these studies, voltage and state-of-charge (SOC) profiles are created based on a flight plan using an equivalent circuit model to check if the flight mission can be completed. Because we are not performing flight testing, in this paper we consider a simpler, theoretical battery model [19] that can support eVTOL operations.

关于飞机电动电池放电模型的现有文献有限。在 [16-18] 中，基于飞行测试提出了电动翼飞机的电池建模和预测。在这些研究中，根据飞行计划使用等效电路模型创建了电压和荷电状态 (SOC) 剖面，以检

Received 11 July 2019; revision received 22 October 2019; accepted for publication 3 December 2019; published online 27 December 2019.

收到日期:2019 年 7 月 11 日；修订收到日期:2019 年 10 月 22 日；接受发表日期:2019 年 12 月 3 日；在线发表日期:2019 年 12 月 27 日。

*M.Sc. Student, Department of Control and Operations, Faculty of Aerospace Engineering, Kluyverweg 1.

* 硕士学位研究生，航空航天工程系控制与运营部门，Kluyverweg 1 号。

† Assistant Professor, Department of Control and Operations, Faculty of Aerospace Engineering, Kluyverweg 1.

† 副教授，航空航天工程系控制与运营部门，Kluyverweg 1 号。

‡ Assistant Professor, Department of Aerospace Engineering,2333 Howe Hall. Senior Member AIAA.

‡ 副教授，航空航天工程系，2333 Howe Hall。美国航空宇航学会资深会员。

查是否可以完成飞行任务。由于我们不会进行飞行测试，在本文中我们考虑了一个更简单的、理论上的电池模型 [19]，该模型可以支持 eVTOL 运营。

This research extends the arrival scheduling models from previous work to a rolling-horizon, eVTOL arrivals sequencing and scheduling at a double-landing-pad vertiport. We analyze our proposed model using a 1-day operations demand corresponding to a hexagonal vertiport network in Houston, TX.

本次研究将前作中的到达调度模型扩展为滚动时间窗口模型，研究了在具有两个着陆垫的立体港口的 eVTOL(电动垂直起降飞机) 到达序列和调度问题。我们使用休斯顿，德克萨斯州的一个六边形立体港口网络在 1 天的运营需求下，分析了我们提出的模型。

III. Model Formulation

III. 模型构建

In this section, we first introduce a generic airspace structure for eVTOL arrivals at a vertiport with two landing pads. Next, we propose an optimization model for a rolling-horizon eVTOL arrivals at a vertiport with two landing pads. In doing so, we make use of a flight dynamics model for eVTOLs equipped with one electric battery and a model for the SOC of an electric battery.

在本节中，我们首先为具有两个着陆垫的立体港口的 eVTOL 到达引入了一种通用空域结构。接着，我们为具有两个着陆垫的立体港口的 eVTOL 到达提出了一种优化模型。在此过程中，我们利用了一种配备单块电池的 eVTOL 飞行动力学模型以及一个描述电池剩余电量的模型。

Lastly, we analyze our optimization model by means of an eVTOL arrival demand model corresponding to a use case of hexagonal vertiport network in Houston, TX. This use case and its operational concept are described in [20].

最后，我们通过一个与休斯顿，德克萨斯州的六边形立体港口网络使用案例相对应的 eVTOL 到达需求模型来分析我们的优化模型。该使用案例及其运营概念在文献 [20] 中有所描述。

In this paper, we consider only eVTOL arrival operations and assume that the two landing pads are used for arrivals only. However, our scheduling model is generic and could be extended to departure operations or mixed operations with departures and arrivals. Another operational assumption is continuous descent approach plus a final vertical landing. This consideration is due to operational safety, to avoid vortex ring state, and energy efficiency [21]. Finally, our approach is applicable for other eVTOL aircraft types, as long as new flight dynamics and battery model are provided.

在本文中，我们仅考虑 eVTOL 到达操作，并假设两个着陆垫仅用于到达。然而，我们的调度模型是通用的，可以扩展到出发操作或混合操作，包括出发和到达。另一个运营假设是连续下降进近加上最终的垂直着陆。这种考虑是为了运营安全，避免涡环状态，并提高能源效率 [21]。最后，只要提供新的飞行动力学和电池模型，我们的方法也适用于其他类型的 eVTOL 飞机。

A. Airspace Structure for eVTOL Arrivals at a Vertiport

A. 立体港口 eVTOL 到达的空域结构

According to [20, 22, 23] and above assumptions, we consider eVTOLs arriving at a vertiport with two landing pads. We assume two arrival and two departure metering fixes [22] located on a radius, r , from the vertiport (see Fig. 1). The metering fixes are the entrance and exit "gates" to enforce time-based separation. The main use of the arrival approach fixes is to funnel traffic and, most important, to push the delay absorption to an area with lower traffic density, further away from the vertiport. We note, however, that the geometry in Fig. 1, that is, the location of the approach fixes on the circle of radius r around the vertiport and the values for R and r , does not affect the formulation of the scheduling model, but only the values of the time-to-fly to an approach fix and vertiport, which influence the numerical results of the scheduling model.

根据 [20, 22, 23] 和以上假设，我们考虑 eVTOL 降落在带有两个着陆垫的立体港口。我们假设有两个到达和两个出发的计量修正点 [22]，位于距离立体港口 r 的半径上的圆周 (见图 1)。计量修正点是实施基于时间的分离。到达方法修正点的主要用途是疏导流量，最重要的是，将延迟吸收到流量密度较低的区域，远离立体港口。然而，图 1 中的几何形状，即修正点位于立体港口周围的半径 r 圆上的修正点，以及 R 和 r 的值，不影响调度模型的公式，但仅影响飞行时间的结果。

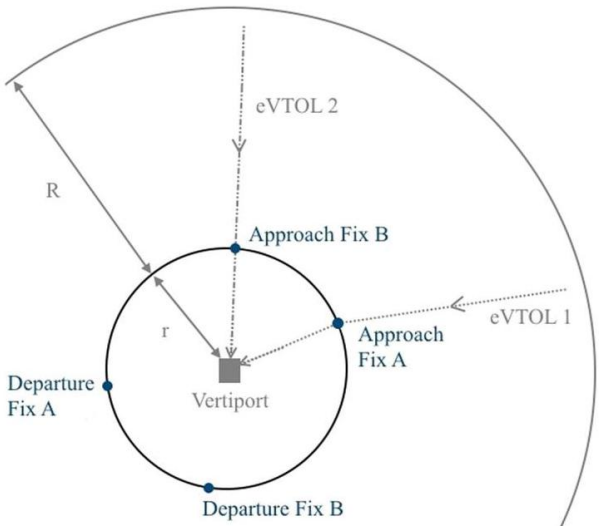

Fig. 1 Airspace structure for eVTOL arrivals at a vertiport with 2 landing pads-top view.

图 1 立体港口空中结构图 2。

Arrivals are initiated on a radius, R , from the approach fixes. In this paper, we consider only two arrival fixes, referred to as approach fixes A and B . The distance between the arrival approach fixes is determined as follows. We assume that the final approach area is circular and has a radius of 400 m . Then the approach fixes are spaced around the vertiport by a quarter of the final approach area circumference. eVTOLs arriving through fix $A\,(B)$ land at a corresponding landing pad $A\,(B)$, independently of the arrivals at the other fix and landing pad. The arrival flow from approach fix A is separated by a distance, s , from the flow from approach fix B (see Fig. 2). Moreover, consecutive arrivals at an approach fix and its corresponding landing pad are separated by Δt_{sep} time units. The flights up to the approach fixes consist of a cruise phase followed by a continuous shallow descent phase (see Fig. 2). Continuous shallow descents are selected for energy efficiency and delay absorption [21]. After reaching one of the two approach fixes (see Fig. 2), an arriving eVTOL flies a horizontal flight segment of length $\bar{d}$, followed by a vertical descent of altitude h .

起飞点在半径 R 上开始，从进近修正点出发。在本文中，我们仅考虑两个起飞修正点，分别称为进近修正点 A 和 B 。起飞修正点之间的距离确定如下。我们假设最后的进近区域是圆形的，半径为 400 m 。然后，进近修正点围绕垂直机场分布，间隔为最后进近区域周长的四分之一。通过修正点 $A\,(B)$ 到达的 eVTOL 在相应的着陆垫 $A\,(B)$ 上着陆，独立于其他修正点和着陆垫上的到达。来自进近修正点 A 的到达流与来自进近修正点 B 的到达流相隔距离 s (见图 2)。此外，进近修正点及其相应着陆垫上的连续到达间隔为 Δt_{sep} 时间单位。到达修正点的航班包括一段巡航阶段，随后是连续的浅降阶段 (见图 2)。选择连续的浅降是为了提高能源效率和延迟吸收 [21]。到达两个进近修正点中的一个后 (见图 2)，到达的 eVTOL 飞行一段水平飞行段，长度为 $\bar{d}$ ，然后是垂直下降，高度为 h 。

The structure of the arrival airspace above considers the flight performances of EHANG 184 [23]. Taking into account a possible shallow descent for EHANG 184 up to the approach fixes, we consider $R = 3500$ m . We also assume a minimum separation $\Delta t_{\text{sep}} = 90$ s between consecutive arrivals to ensure a minimum lateral separation of 1000ft or 305 m [20]. This also avoids that two or more eVTOLs are at the same time in the vertical flight phase. Moreover, it ensures that there is sufficient time for landing pad clearance.

考虑到的到达空域结构考虑了 EHANG 184 的飞行性能 [23]。考虑到 EHANG 184 可能的浅降直到进近修正点，我们考虑 $R = 3500$ m 。我们还假设连续到达之间的最小间隔 $\Delta t_{\text{sep}} = 90$ s ，以确保最小横向间隔为 1000ft 或 305 m [20]。这还可以避免两个或更多的 eVTOL 同时处于垂直飞行阶段。此外，这确保了有足够的时间进行着陆垫的清理。

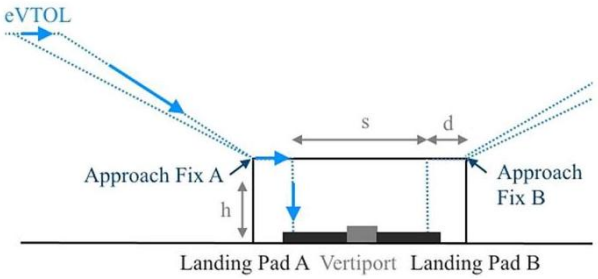

Fig. 2 Airspace structure for eVTOL arrivals at a vertiport with 2 landing pads-side view.

图 2 电子起降场中 eVTOL 飞机降落的空域结构，带有 2 个着陆垫 - 侧视图。

The radius $r = 400$ m and $s = 530$ m follow from having $\Delta t_{\text{sep}} = 90$ s and an average eVTOL horizontal speed of 5.9 m/s during the final approach. The distance $d = 135$ m follows from the values assumed for r and s . Lastly, $h = 200$ m allows for a maximum eVTOL shallow descent from a cruise altitude of 500 m [23] and ensures clearance from high-rise buildings.

半径 $r = 400$ m 和 $s = 530$ m 由拥有 $\Delta t_{\text{sep}} = 90$ s 以及在最后进近阶段平均 eVTOL 水平速度 5.9 m/s 得出。距离 $d = 135$ m 由 r 和 s 的假定值得出。最后，$h = 200$ m 允许 eVTOL 从巡航高度 500 m [23] 进行最大浅降，并确保与高层建筑保持安全距离。

B. eVTOL Flight Dynamics Model

B. eVTOL 飞行动力学模型

We consider the following flight dynamics model for EHANG 184 multirotor eVTOL [23], which is equipped with one electric battery:

我们考虑以下 EHANG 184 多旋翼 eVTOL [23] 的飞行动力学模型，该模型配备有一个电动电池:

$$P_r = P_i + P_a + P_c + P_f = 4 \cdot T \cdot v_i + T \cdot V \cdot \sin\alpha + 0.2 \cdot P_r \tag{1}$$

$$V = \sqrt{V_x^2 + V_h^2} \tag{2}$$

$$\alpha = \theta + \gamma = \theta + \arctan\left(\frac{V_x}{V_h}\right) \tag{3}$$

$$v_h = \sqrt{\frac{T_r}{2\rho\pi R^2}} \tag{4}$$

$$v_i = \frac{v_h^2}{\sqrt{\left(V \cdot \cos\left(\alpha\right)\right)^2 + \left(V \cdot \sin\left(\alpha\right) + v_i\right)^2}} \tag{5}$$

where P_r, P_i, P_a, P_c, P_f are the required, induced, parasite, climb, and profile power, respectively, with $P_f = 0.2P_r$ [24] ; V is the true airspeed with the vertical component V_x and the horizontal component V_h; $T, \alpha, \theta, \gamma$ are the thrust, the angle of attack, the pitch angle, and flight path angle, respectively; and also, v_i, v_h, R, T_r, ρ are the induced velocity, the induced velocity in hover, rotor radius, thrust per rotor, and the air density, respectively. Here, ρ is assumed to be equal to the international standard atmosphere density at sea level. We further assume that all rotors produce equal thrust. Thus, we assume an upper and lower rotor to produce equal thrust such that $T_r = (1/8)\,T$. Lastly, the induced velocity v_i in Eq. (5) follows from the momentum theory and the induced velocity in hover, denoted by v_h .

其中 P_r, P_i, P_a, P_c, P_f 分别是所需的、诱导的、阻力的、爬升的和轮廓功率，$P_f = 0.2P_r$ [24] ; V 是真实空速，其垂直分量为 V_x ，水平分量为 V_h; $T, \alpha, \theta, \gamma$ 分别是推力、攻角、俯仰角和飞行路径角；此外，v_i, v_h, R, T_r, ρ 分别是诱导速度、悬停时的诱导速度、旋翼半径、每个旋翼的推力和空气密度。这里，ρ 假设等于国际标准海平面大气密度。我们还假设所有旋翼产生相等的推力。因此，我们假设上旋翼和下旋翼产生相等的推力，使得 $T_r = (1/8)\,T$ 。最后，方程 (5) 中的诱导速度 v_i 由动量理论和悬停时的诱导速度 v_h 得出。

C. Electric Battery State-of-Charge

C. 电动电池充电状态

We consider the following model for the total electric power demand, P_d [18, 19] :
我们考虑以下总电功率需求 P_d [18, 19] 的模型:

$$P_d = \mathrm{SF} \cdot \frac{1}{\eta_P} \frac{1}{\eta_e} P_r \tag{6}$$

where SF = 1.5 is a safety factor to account for potential adverse weather conditions and the need for emergency diversion, η_P is the rotor efficiency ($\eta_P = 0.7652$) , and η_e is the mechanical efficiency ($\eta_e = 0.85$) . We further consider the following model [19] for the battery SOC demand during a flight phase k that starts at time t_0^k and ends at time $t_f^k, 1 \leq k \leq 4$, where $k = 1$ corresponds to the cruise phase, $k = 2$ corresponds to the shallow descent phase, $k = 3$ corresponds to the horizontal final approach, and $k = 4$ corresponds to the vertical final approach:
其中 SF = 1.5 是安全系数，用于考虑潜在的恶劣天气条件以及紧急偏航的需要，η_P 是转子效率 ($\eta_P = 0.7652$) ，η_e 是机械效率 ($\eta_e = 0.85$) 。我们还进一步考虑了以下模型 [19]，用于飞行阶段电池 SOC 需求的计算，该阶段开始于时间 t_0^k ，结束于时间 $t_f^k, 1 \leq k \leq 4$ ，其中 $k = 1$ 对应巡航阶段，$k = 2$ 对应浅降阶段，$k = 3$ 对应水平最后进近阶段，$k = 4$ 对应垂直最后进近阶段:

$$I(k) = \frac{P_d(k)}{V_n} \tag{7}$$

$$\mathrm{SOC}(k) = \frac{I(k) \cdot \left(t_f^k - t_0^k\right)}{3600 \cdot Q} \tag{8}$$

$$\mathrm{SOC} = \sum_{k=1}^{4} \mathrm{SOC}(k) \tag{9}$$

where $I(k)$ is the total current of all battery cells during flight phase k , $1 \leq k \leq 4$; V_n is the nominal battery voltage; and Q is the battery capacity. The battery is assumed to be empty if it reaches a 10% SOC, to prevent it from deep discharge. We use this battery model and the flight dynamics model in Sec. III.B to limit the latest possible landing time RTA_l . This hard constraint ensures that each aircraft lands before its SOC drops below 10% .
其中 $I(k)$ 是飞行阶段所有电池单元的总电流 k ，$1 \leq k \leq 4$; V_n 是电池的标称电压；Q 是电池容量。假设电池在达到 10% SOC 时为空，以防止其过度放电。我们使用这个电池模型和第 III.B 节中的飞行动力学模型来限制最晚可能的着陆时间 RTA_l 。这个硬约束确保每架飞机在 SOC 降至 10% 之前着陆。

D. Rolling-Horizon eVTOL Arrival Sequencing and Scheduling at a Vertiport

D. 竖直起降机场的电动垂直起降飞机到达顺序和调度

Using the airspace structure in Sec. III.A, the flight dynamics model for an eVTOL in Sec. III.B, and the eVTOL battery model in Sec. III.C, in this section we propose an optimal, rolling-horizon sequencing and scheduling algorithm for eVTOL arrivals at a verti-port. We also take into account the possibility for eVTOLs to hover at a distance $R + r$ away from the vertiport. Here, hovering is seen as an additional possibility to impose delay on eVTOLs when the arrival rate is larger than the landing rate of the eVTOLs at the vertiport, that is, the delay imposed on eVTOLs is too large to be absorbed by means of shallow descent. The objective of this optimization model is to minimize the total time deviation of arriving eVTOLs from their preferred time of arrival. Next we define the preferred eVTOL times of arrival.
使用第三节 A 部分中的空域结构、第三节 B 部分中的 eVTOL 飞行动力学模型以及第三节 C 部分中的 eVTOL 电池模型，在本节中我们提出了一个最优的、滚动时间窗口的排序和调度算法，用于 eVTOL 在立体港口的到达。我们还考虑了 eVTOL 在距离立体港口 $R + r$ 的位置悬停的可能性。在这里，悬停被视为当 eVTOL 的到达率大于立体港口的着陆率时，对 eVTOL 施加延迟的额外可能性，即对 eVTOL 施加的延迟太大，无法通过浅降方式吸收。该优化模型的目标是最小化到达的 eVTOL 与其期望到达时间的总时间偏差。接下来我们定义了 eVTOL 的期望到达时间。

First, given the airspace structure in Sec. III.A and the eVTOL flight dynamics in Sec. III.B, we determine, for a given RTA at the vertiport, an optimal eVTOL arrival trajectory with respect to energy consumption. These optimal arrival trajectories are computed using the GPOPS-II software [25]. For a given RTA, the output of GPOPS-II is an optimal eVTOL arrival trajectory, which is defined by the state variables (V_x, V_h , altitude, and distance), the control variables (T and θ), and the total energy required to fulfill the trajectory.

首先，考虑到第三节 A 部分中的空域结构和第三节 B 部分中的 eVTOL 飞行动力学，对于给定的立体港口的 RTA，我们确定了一个最优的 eVTOL 到达轨迹，以降低能量消耗。这些最优到达轨迹是使用 GPOPS-II 软件 [25] 计算得出的。对于给定的 RTA，GPOPS-II 的输出是一个最优的 eVTOL 到达轨迹，该轨迹由状态变量 (V_x, V_h (包括速度、高度和距离)、控制变量 (T 和 θ ，以及完成轨迹所需的总能构成。

Next, we use the GPOPS-II output to determine the required power P_r at each flight phase $k, 1 \leq k \leq 4$, of the eVTOL arrival trajectory (see also Sec. III.B). Further, P_r is used to determine the battery power demand P_d and the SOC demand for the eVTOL battery (see Sec. III.C). We determine a feasible set of RTAs based on the remaining SOC of the eVTOLs, the minimum required SOC to reach the vertiport at these RTAs, and the flight performance of the eVTOLs. The minimum RTA in the feasible set corresponds to the earliest possible time that the eVTOL can arrive at the vertiport. The maximum RTA in the feasible set is determined by the SOC of the eVTOL battery. The RTA obtained with the minimum energy consumption, which we refer to as the estimated time of arrival (ETA), is the preferred arrival time of an eVTOL at the vertiport.

接下来，我们使用 GPOPS-II 输出来确定每个飞行阶段 P_r 的 eVTOL 到达轨迹所需的功率 $k, 1 \leq k \leq 4$ (也见第 III.B 节)。此外，P_r 还用于确定 eVTOL 电池的功率需求 P_d 和 SOC 需求 (见第 III.C 节)。我们根据 eVTOL 的剩余 SOC、在这些 RTA 到达垂直港口所需的最小 SOC 以及 eVTOL 的飞行性能，确定一组可行的 RTA。在可行集中的最小 RTA 对应于 eVTOL 能够到达垂直港口的最早可能时间。可行集中最大的 RTA 由 eVTOL 电池的 SOC 决定。使用最小能量消耗获得的 RTA，我们称之为预计到达时间 (ETA)，是 eVTOL 在垂直港口偏好的到达时间。

Having obtained a set of feasible RTAs for arriving eVTOLs, we next introduce a rolling-horizon optimization model that sequences and schedules a set of G eVTOLs arriving at a vertiport such that the total time deviation from their ETAs, that is, $\sum_{i \in G} |\mathrm{RTA}_i - \mathrm{ETA}_i|$, is minimized. The rolling-horizon [5,26] consists of planning periods of 15 min and a total planning horizon of 30 min , that is,2 planning periods (see Fig. 3). In each planning horizon, we find the eVTOL RTAs that result in a minimal total time deviation from their ETAs. We freeze the RTAs of the eVTOLs in the first planning period, that is, during the first 15 min . We also save the last RTA in this period, for each landing pad $\mathrm{RTA}_{\mathrm{last},lp}(i), i \in \{A, B\}$. We further shift the planning horizon by 15 min and optimize the arrival time of the remaining eVTOLs. We also ensure minimum separation between the time of the last eVTOL arrival in the previous planning period and the first eVTOL arrival in the next planning period.

获得一组可行的到达 eVTOL 的 RTAs 后，我们接下来引入一个滚动窗口优化模型，该模型为到达立体港口的一组 G eVTOL 排序和调度，以使得它们从预计到达时间 (ETA) 的总时间偏差，即 $\sum_{i \in G} |\mathrm{RTA}_i - \mathrm{ETA}_i|$ 最小化。滚动窗口 [5,26] 包括计划周期为 15 min 和总计划范围为 30 min 的计划期，即 2 个计划周期 (见图 3)。在每个计划周期内，我们找到导致从 ETA 的最小总时间偏差的 eVTOL RTAs。我们固定第一个计划周期内 eVTOL 的 RTAs，即在第一个 15 min 期间。我们还保存这个周期中每个着陆点的最后一个 RTA $\mathrm{RTA}_{\mathrm{last},lp}(i), i \in \{A, B\}$ 。然后我们将计划范围向前移动 15 min ，并优化剩余 eVTOL 的到达时间。我们还确保前一个计划周期中最后一个 eVTOL 到达时间和下一个计划周期中第一个 eVTOL 到达时间之间有最小间隔。

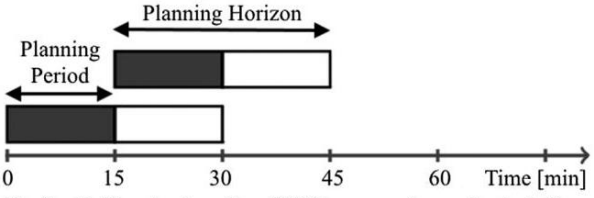

Fig. 3 Rolling-horizon for eVTOL sequencing and scheduling.

1. Decision Variables

1. 决策变量

We optimize the values of the following decision variables: time between the approach fix $i, i \in \{A, B\}$, and the vertiport. The fourth term penalizes the time the eVTOL spends hovering at distance $R+r$ from the vertiport. Further, $c_e^p, c_l^p, c_{l,af}^p, c_{l,h}^p$ are the cost coefficients corresponding to the four penalty terms above, where $c_e^p, c_l^p, c_{l,af}^p, c_{l,h}^p$ are derived from the power required to absorb the assigned time deviation of an eVTOL from its ETA.

我们优化以下决策变量的值: 从进近定位点到立体港口之间的时间 $i, i \in \{A, B\}$ 。第四项对 eVTOL 在距离立体港口 $R + r$ 处悬停的时间进行惩罚。此外，$c_e^p, c_l^p, c_{l,af}^p, c_{l,h}^p$ 是上述四个惩罚项对应的成本系数，其中 $c_e^p, c_l^p, c_{l,af}^p, c_{l,h}^p$ 来自于吸收 eVTOL 从其 ETA 分配的时间偏差所需的功率。

$$a^p = \begin{cases} 1, & \text{if eVTOL } p \text{ flies through approach fix } A, \\ 0, & \text{if eVTOL } p \text{ flies through approach fix } B, \end{cases}$$

$$z^{pq} = \begin{cases} 1, & \text{if eVTOL } p \text{ and eVTOL } q \text{ fly through the same approach fix,} \\ 0, & \text{otherwise} \end{cases}$$

$$s^{pq} = \begin{cases} 1, & \text{if eVTOL } p \text{ arrives prior to eVTOL } q, \\ 0, & \forall p \in G, q \in [p-K, p+K], p \neq q, \end{cases} \quad \forall p \in G, \text{ where } K \in \mathbb{N}^+ \text{ is}$$

the maximum number of position shifts from the first-come-first-served (FCFS) arrival sequence [27].
从先来先服务 (FCFS) 到达序列中的最大位置偏移次数 [27]。
Δt_e^p = Amount of time eVTOL p is scheduled beforeits
Δt_e^p = eVTOL p 在其预计到达时间之前预定的时间量

$$\text{ETA}^p(i), i \in \{A, B\} \text{ , i.e.,}$$

$$\text{ETA}^p(i) - \text{RTA}^p(i), \forall p \in G, \Delta t_e^p \geq 0$$

Δt_l^p = Delay assigned to eVTOL p in shallow descent, that is, amount of time eVTOL p is scheduled after its
Δt_l^p = 分配给 eVTOL p 在浅降过程中的延迟，即 eVTOL p 在其

$$\text{ETA}^p(i), i \in \{A, B\} \text{ , i.e., } \text{RTA}^p(i) - \text{ETA}^p(i) \text{ ,}$$

$$\forall p \in G, \Delta t_l^p \geq 0$$

$\Delta t_{l,h}^p$ = Delay assigned to eVTOL p in hover at distance $R + r$ from the vertiport, that is, amount of time
$\Delta t_{l,h}^p$ = 分配给 eVTOL p 在距离机场 $R + r$ 的悬停中的延迟，即时间量

$$\text{eVTOL } p \text{ is scheduled after its } \text{ETA}^p(i), i \in \{A, B\} \text{ ,}$$

$$\text{i.e., } \text{RTA}^p(i) - \text{ETA}^p(i), \forall p \in G, 0 \leq \Delta t_{l,h}^p \leq \Delta t_{l,h,\max}^p$$

where $\Delta t_{l,h,\max}^p$ is determined from the remaining battery SOC.
其中 $\Delta t_{l,h,\max}^p$ 由剩余电池 SOC 确定。

2. Objective Function

2. 目标函数

The total time deviations from the ETAs of the eVTOLs arriving at the vertiport are minimized, that is,
优化 eVTOL 到达机场的预计到达时间 (ETA) 的总时间偏差，即

$$\min \sum_{p \in G} c_e^p \cdot \Delta t_e^p + c_l^p \cdot \Delta t_l^p + c_{l,af}^p \cdot a^p$$

$$\cdot \left(\Delta t_{l,A}^{p} - \Delta t_{l,B}^{p}\right) + c_{l,h}^{p} \cdot \Delta t_{l,h}^{p}, \quad \text{where} \tag{10}$$

$$\Delta t_{l,i}^{p} = \max\left(0, \left(\mathrm{ETA}^{p}\left(i\right) + T_{t}^{p}\left(i\right) - \mathrm{ETA}^{p}\left(j\right) - T_{t}^{p}\left(j\right)\right)\right)$$

$$\forall i, j \in \{A, B\}, i \neq j \tag{11}$$

The first term in Eq. (10) penalizes the amount of time eVTOLs arrive at the vertiport before their ETA. The second term penalizes the delay assigned to eVTOLs in shallow descent. The third term penalizes the additional flight time resulting from selecting an approach fix $i, i \in \{A, B\}$, which needs more time to reach, that is, requires a longer arrival trajectory, than the other approach fix $j, j \in \{A, B\}$, $i \neq j$. The delay resulting from choosing an approach fix, that is, $\Delta t_{l,i}^{p}$, $i \in \{A, B\}$, is calculated using Eq. (11), where $T_{t}^{p}\left(i\right)$ is the flight 3. Constraints

方程 (10) 中的第一项对 eVTOL 在 ETA 之前到达机场的时间进行惩罚。第二项对分配给 eVTOL 在浅降过程中的延迟进行惩罚。第三项对选择一个进近修正点 $i, i \in \{A, B\}$ 产生的额外飞行时间进行惩罚，这个点需要更多时间到达，即，需要一个更长的到达轨迹，比另一个进近修正点 $j, j \in \{A, B\}$ ，$i \neq j$ 。选择进近修正点的延迟，即 $\Delta t_{l,i}^{p}$ ，$i \in \{A, B\}$ ，使用方程 (11) 计算，其中 $T_{t}^{p}\left(i\right)$ 是飞行

We require the following set of constraints to be satisfied:

我们要求满足以下一组约束条件:

$$s^{pq} + s^{qp} = 1, \ \forall p, q \in G \tag{12}$$

$$z^{pq} = z^{qp}, \ \forall p, q \in G \tag{13}$$

$$z^{pq} \geq a^{p} + a^{q} - 1, \ \forall p, q \in G, p \neq q \tag{14}$$

$$z^{pq} \geq -a^{p} - a^{q} + 1, \ \forall p, q \in G, p \neq q \tag{15}$$

$$z^{pq} \leq \frac{1}{2}a^{p} - \frac{1}{2}a^{q} + 1, \ \forall p, q \in G, p \neq q \tag{16}$$

$$z^{pq} \leq -\frac{1}{2}a^{p} + \frac{1}{2}a^{q} + 1, \ \forall p, q \in G, p \neq q \tag{17}$$

$$\mathrm{RTA}_{e}^{p} \leq \mathrm{RTA}^{p} \leq \mathrm{RTA}_{l}^{p}, \ \forall p \in G \tag{18}$$

$$\mathrm{RTA}^{p} \geq \mathrm{RTA}^{q} + \Delta t_{\mathrm{sep}}^{qp} \cdot z^{qp} - M^{pq} \cdot s^{pq}, \ \forall p, q \in G, p \neq q$$

(19)

$$\mathrm{RTA}^{p}\left(i\right) \geq \mathrm{RTA}^{q}\left(i\right) + \Delta t_{\mathrm{sep}}^{qp} \cdot z^{qp} - M^{pq} \cdot s^{pq},$$

$$\forall p, q \in G, p \neq q, i \in \{A, B\} \tag{20}$$

in which

其中

$$\mathrm{RTA}_{e}^{p} = a^{p} \cdot \mathrm{RTA}_{e,lp}^{p}\left(A\right) + \left(1 - a^{p}\right) \cdot \mathrm{RTA}_{e,lp}^{p}\left(B\right) \tag{21}$$

$$M^{pq} = \mathrm{RTA}_{l}^{q} + \Delta t_{l,h,\max}^{p} + \Delta t_{\mathrm{sep}}^{qp} - \min\left(\mathrm{RTA}_{e,lp}^{p}\left(A\right), \mathrm{RTA}_{e,lp}^{p}(B \right. \tag{B}$$

(22)

$$\mathrm{RTA}_{e,lp}^{p}\left(i\right) = \max\left(\mathrm{RTA}_{\ \mathrm{last}\ ,lp}\left(i\right)\right.$$

$$\left. + \Delta t_{\mathrm{sep}}^{pq}, \mathrm{RTA}_{e}^{p}\left(i\right) + T_{t}^{p}\left(i\right)\right), \ \forall i \in \{A, B\} \tag{23}$$

$$\mathrm{RTA}^p = a^p \cdot \left(\mathrm{RTA}^p\left(A\right) + T_t^p\left(A\right)\right) + \left(1 - a^p\right)$$

$$\cdot \left(\mathrm{RTA}^p\left(B\right) + T_t^p\left(B\right)\right) \tag{24}$$

$$\mathrm{RTA}^p\left(i\right) = \mathrm{ETA}^p\left(i\right) + \Delta t_l^p - \Delta t_e^p + \Delta t_{l,h}^p,\ \forall i \in \{A, B\} \tag{25}$$

Constraint (12) ensures that either eVTOL p follows eVTOL q or eVTOL q follows eVTOL p . Equation (13) ensures that if eVTOL p and q go through the same approach fix and to the same landing pad, the reverse is also true. Equations (14) and (15) further define $z^{pq} = 1$ if both eVTOL p and q use approach fix A and B, respectively. Equations (16) and (17) define $z^{pq} = 0$ if eVTOLs p and q fly through different approach fixes. The feasible set of RTAs for landing at the vertiport is described in Eq. (18). The latest RTA_l^p results from the battery model (see Sec. III.C), whereas the earliest possible time of arrival RTA_e^p is computed by Eq. (21). Here, $\mathrm{RTA}_{e,lp}^p\left(i\right)$ is the earliest possible landing time of eVTOL p arriving through approach fix i and thus at landing pad $i, i \in \{A, B\}$. This is derived from the flight performance model (see Sec. III.B). Equations (19) and (20) ensure a time-based separation of at least $\Delta t_{\mathrm{sep}}^{qp}$ only if eVTOL p follows eVTOL q at the same approach fix and, thus, the same landing pad. We consider variable M^{pq} , defined in Eq. (22), which ensures that the time separation between two eVTOLs is enforced only when $s^{pq} = 0$, that is, when eVTOL p arrives at the vertiport after eVTOL q . Equation (23) shows the earliest possible time to arrive at the vertiport based on the last eVTOL arrival time, $\mathrm{RTA}_{\mathrm{last},lp}$, in the previous planning period. Equations (24) and (25) define the RTA for eVTOL p at the selected vertiport landing pad and at approach fix A or B, respectively.

约束条件 (12) 确保 eVTOL p 要么跟随 eVTOL q ，要么 eVTOL q 跟随 eVTOL p 。方程 (13) 确保如果 eVTOL p 和 q 通过相同的进近定位点并降落在同一块着陆板上，那么反过来也成立。方程 (14) 和 (15) 进一步定义了 $z^{pq} = 1$ ，如果 eVTOL p 和 q 分别使用进近定位点 A 和 B。方程 (16) 和 (17) 定义了 $z^{pq} = 0$ ，如果 eVTOL p 和 q 飞越不同的进近定位点。在机场的可行 RTA 集合由方程 (18) 描述。最新的 RTA_l^p 结果来自电池模型 (见第 III.C 节)，而最早可能的到达时间 RTA_e^p 是通过方程 (21) 计算的。在这里，$\mathrm{RTA}_{e,lp}^p\left(i\right)$ 是 eVTOL p 通过进近定位点 i 到达并因此在着陆板 $i, i \in \{A, B\}$ 上着陆的最早可能时间。这是从飞行性能模型 (见第 III.B 节) 推导出来的。方程 (19) 和 (20) 确保仅在 eVTOL p 在同一进近定位点跟随 eVTOL q 时，即在同一块着陆板上，才至少有 $\Delta t_{\mathrm{sep}}^{qp}$ 的时间间隔。我们考虑变量 M^{pq} ，在方程 (22) 中定义，它确保仅在 $s^{pq} = 0$ 时，即 eVTOL p 在 eVTOL q 到达机场后到达时，才执行两个 eVTOL 之间的时间间隔。方程 (23) 显示了基于上一个规划周期中最后一个 eVTOL 到达时间 $\mathrm{RTA}_{\mathrm{last},lp}$ 的最早可能到达机场的时间。方程 (24) 和 (25) 分别定义了在选定机场着陆板上的 eVTOL p 的 RTA 和在进近定位点 A 或 B 的 RTA。

E. eVTOL Arrival Demand Model

E. eVTOL 到达需求模型

We consider the eVTOL arrival demand model introduced in [8], where a prediction for an eVTOL arrival demand distribution over a day is provided for the hub vertiport in an envisioned hexagonal vertiport network of Houston, TX. In [8], the distribution of arrivals is determined as the sum of 3 normal distributions: $N\left(8, 2\right)$ and $N\left(16, 2\right)$ corresponding to commuter rush hour peaks at 8:00 a.m. and 4:00 p.m., respectively, and $N\left(12, 6\right)$ corresponding to daytime commuter travel. The obtained distribution (see Fig. 4) is normalized to a cumulative distribution and scaled by coefficient $M_4 = 8500$ [8] .

我们考虑了文献 [8] 中引入的 eVTOL 到达需求模型，该模型为德克萨斯州休斯顿设想的六边形垂直起降场网络中的枢纽机场提供了一天中 eVTOL 到达需求分布的预测。在文献 [8] 中，到达分布被确定为 3 个正态分布的和: $N\left(8, 2\right)$ 和 $N\left(16, 2\right)$ 分别对应上午 8:00 和下午 4:00 的通勤高峰，以及 $N\left(12, 6\right)$ 对应白天通勤旅行。得到的分布 (见图 4) 被归一化为累积分布，并由系数 $M_4 = 8500$ [8] 进行缩放。

Using the probability distribution function in [8] for eVTOL arrivals at the hub vertiport, we estimate $\lambda\left(t\right)$, the number of arrivals in hour $t, t \in \{0, 1, \ldots, 24\}$. Further, we consider an inhomogeneous Poisson process with rate $\lambda\left(t\right)$ to generate eVTOL interarrival times at the vertiport. Moreover, based on the hexagonal vertiport network structure in [8], we assume that the eVTOLs start their arrival trajectory from one of 6 equally spaced, origin points on a circle of radius $R + r$ (see Fig. 5). Each eVTOL has probability 1/6 of originating from one of the 6 origin points on the circle.

使用文献 [8] 中给出的枢纽机场 eVTOL 到达的概率分布函数，我们估计了 $\lambda\left(t\right)$ ，即小时 $t, t \in \{0, 1, \ldots, 24\}$ 内的到达数量。此外，我们考虑了一个速率 $\lambda\left(t\right)$ 的非齐次泊松过程来生成垂直起降场的

eVTOL 到达间隔时间。基于文献 [8] 中的六边形垂直起降场网络结构，我们假设 eVTOL 从半径为 $R+r$ 的圆上 6 个等间距的起点之一开始它们的到达轨迹 (见图 5)。每个 eVTOL 从圆上的 6 个起点之一出发的概率为 1/6 。

Now, let an eVTOL $p+1$ arriving at an approach fix $i, i \in \{A, B\}$, be preceded by eVTOL p . Then, the expected time of arrival of eVTOL $p+1$ at an approach fix $i, \mathrm{ETA}\,(i)^{p+1}$, is determined in Eq. (26), where S is the interarrival time between eVTOL $p+1$ and eVTOL p , and $\Delta t_{l,i}^{p}$ is the additional flight time due to selecting approach fix i , which results in a longer arrival trajectory than selecting the other approach fix [see also Eq. (11)].

现在，假设一个 eVTOL $p+1$ 正在接近定位点 $i, i \in \{A, B\}$ 到达，前面有 eVTOL p 。那么，eVTOL $p+1$ 在接近定位点 $i, \mathrm{ETA}\,(i)^{p+1}$ 的预计到达时间由公式 (26) 确定，其中 S 是 eVTOL $p+1$ 和 eVTOL p 之间的到达间隔时间，$\Delta t_{l,i}^{p}$ 是由于选择接近定位点 i 而增加的飞行时间，这导致了一个比选择其他接近定位点更长的到达轨迹 (也见公式 (11))。

$$\mathrm{ETA}\,(i)^{p+1} = \mathrm{ETA}\,(i)^{p} + S + \Delta t_{l,i}^{p} \tag{26}$$

where $S \sim \exp\left(\lambda\left(t\right)\right), i \in \{A, B\}$.

其中 $S \sim \exp\left(\lambda\left(t\right)\right), i \in \{A, B\}$ 。

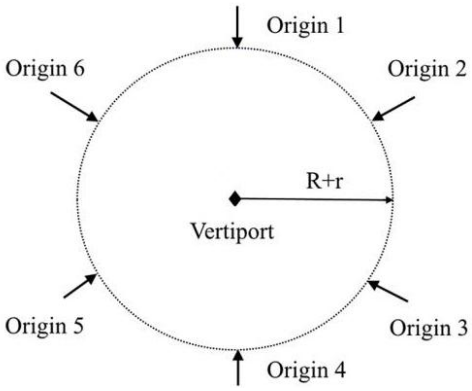

Fig. 5 Origin points for eVTOL arrivals at a hub vertiport.

图 5 eVTOL 在枢纽型立体港的到达原点。

Lastly, we assume that the initial SOC of an eVTOL p follows a normal distribution $N\left(30, 5\right)$, where a mean initial SOC battery of 30% allows for all trajectories with an RTA in the feasible set of RTAs (see Sec. III.D) to be fulfilled.

最后，我们假设 eVTOL p 的初始 SOC 遵循正态分布 $N\left(30, 5\right)$ ，其中平均初始 SOC 电池的 30% 能够满足所有在可行 RTA 集合 (见第 III.D 节) 中的 RTA 轨迹。

IV. Results

IV. 结果

In this section we present the arrival sequencing and scheduling results for an EHANG 184 [23]. In Sec. IV.A we illustrate the energy consumption achieved by EHANG 184 for various RTAs and shallow descents. In Sec. IV.B we show the arrival delay for EHANG 184 for a rolling-horizon arrival sequencing and scheduling for 1 day of operations. In Sec. IV.C we discuss the distribution of EHANG 184 delays based on Monte Carlo simulation of a 1-day operations demand.

在本节中，我们展示了 EHANG 184 的到达顺序和调度结果。在第 IV.A 节中，我们说明了 EHANG 184 在不同 RTA 和浅降过程中的能耗。在第 IV.B 节中，我们展示了 EHANG 184 在滚动窗口到达顺序和调度下一天的运营中的到达延误。在第 IV.C 节中，我们基于一天运营需求的蒙特卡洛模拟讨论了 EHANG 184 延误的分布。

A. Energy-Optimal Arrival Trajectory for a Single eVTOL

A. 单个 eVTOL 的能量最优到达轨迹

In this section we determine, using the GPOPS-II trajectory optimizer and the flight dynamics model in Sec. III.B, the energy optimal arrival trajectories for a given set of RTAs at a given approach fix. The cruise phase is performed at 500 m altitude and 27.8 m/s cruise speed [23]. The eVTOL arrival scheduling and sequencing is initiated at $R + \bar{r} = 3900$ m distance from the vertiport (see Sec. III.A). A shallow descent is initiated between 3400 and 1000 m from the vertiport at a constant horizontal velocity $V_h = 5.9$ m/s and variable vertical velocity V_x . After passing the approach fix, a horizontal flight phase is executed at velocity $V_h = 5.9$ m/s and a vertical flight phase at velocity $V_x = 2.9$ m/s .

在本节中，我们使用 GPOPS-II 轨迹优化器和第 III.B 节中的飞行动力学模型，确定了一组给定的 RTA 在给定的进近定位点处的能量最优到达轨迹。巡航阶段在 500 m 高度和 27.8 m/s 巡航速度 [23] 下进行。eVTOL 到达调度和排序从距离垂直机场 $R + \bar{r} = 3900$ m 的位置开始 (参见第 III.A 节)。在距离垂直机场 3400 到 1000 m 的位置，以恒定的水平速度 $V_h = 5.9$ m/s 和可变的垂直速度 V_x 开始浅降。通过进近定位点后，执行水平飞行阶段，速度为 $V_h = 5.9$ m/s ，垂直飞行阶段的速度为 $V_x = 2.9$ m/s 。

Figure 6 shows the energy-optimal eVTOL arrival trajectories for given RTAs at the approach fix, RTA_{af} . For a large RTA_{af} , the eVTOLs spend this large time flying a more shallow descent. An $\text{RTA}_{af} = 165$ s is the shortest possible time to reach an approach fix, given the flight performance of EHANG 184 [23]. For $165 \text{ s} \leq \text{RTA}_{af} \leq 525$ s , the eVTOL is required to arrive at the double-landing-pad vertiport at $262 \text{ s} \leq RTA \leq 622$ s because the flight time between the approach fix and vertiport is 97 s . A trajectory with $\text{RTA}_{af} = 165$ s also corresponds to the minimum energy required to reach the approach fix. This trajectory with $\text{RTA}_{af} = 165$ s is used as a baseline trajectory to determine the eVTOLs ETAs at the vertiport, which are an input for the sequencing and scheduling model.

图 6 显示了在进近定位点处给定 RTA 的能量最优 eVTOL 到达轨迹 RTA_{af} 。对于较大的 RTA_{af} ，eVTOL 在这个较大的时间内进行较浅的下降飞行。一个 $\text{RTA}_{af} = 165$ s 是在 EHANG 184 的飞行性能 [23] 下，到达进近定位点的最短可能时间。对于 $165 \text{ s} \leq \text{RTA}_{af} \leq 525$ s ，eVTOL 需要到达具有双降落垫的垂直机场 $262 \text{ s} \leq RTA \leq 622$ s ，因为从进近定位点到垂直机场的飞行时间为 97 s 。具有 $\text{RTA}_{af} = 165$ s 的轨迹还对应于到达进近定位点所需的最小能量。这个具有 $\text{RTA}_{af} = 165$ s 的轨迹被用作基线轨迹，以确定 eVTOL 在垂直机场的预计到达时间 (ETA)，这是排序和调度模型的输入。

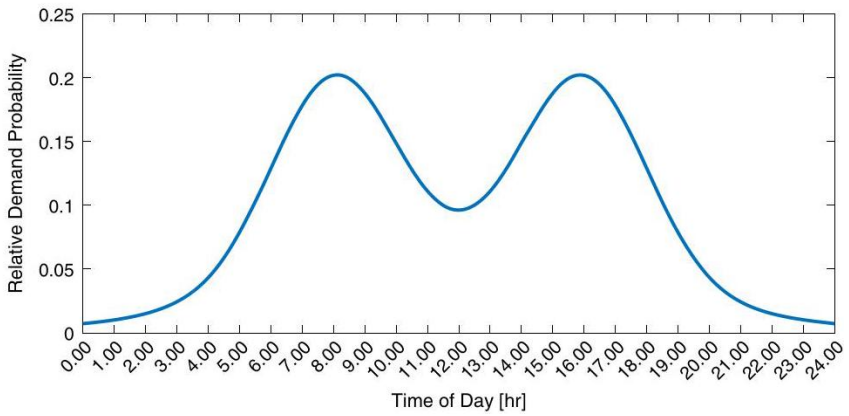

Fig. 4 Demand probability distribution function for eVTOL arrivals at a hub vertiport [8].
图 4 显示了 eVTOL 在中心垂直机场到达的需求概率分布函数 [8]。

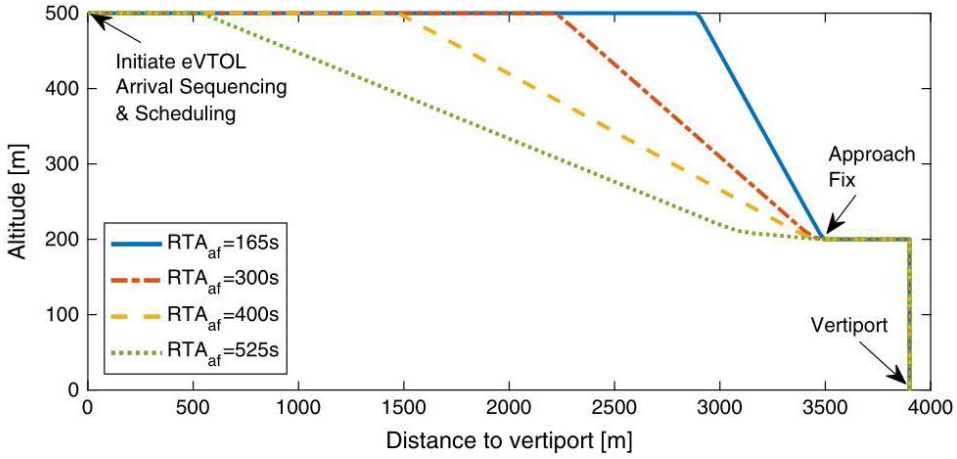

Fig. 6 EHANG 184 energy-optimal eVTOL arrival trajectory for different RTAs to approach fix.

图 6 显示了 EHANG 184 在不同 RTA 下到达进近定位点的能量最优 eVTOL 到达轨迹。Please note that the placeholders like '[latex0]', '[latex1]', etc., have been retained as per the instructions.

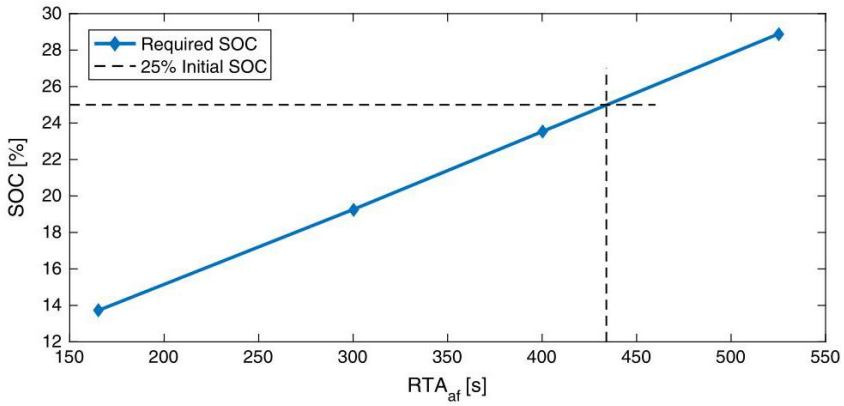

Fig. 7 Required SOC for different RTAs at approach fix.

图 7 显示了在不同进近定位点执行图 6 中每条轨迹所需的 SOC。

Figure 7 shows the SOC required to perform each of the trajectories in Fig. 6, based on the battery model in Sec. III.C. We assume a battery capacity $Q = 5000$ Ahr and a nominal voltage $V_n = 12$ V . Figure 7 shows, for instance, that for a remaining SOC = 25% , the latest RTA at the approach fix is $\text{RTA}_{af} = 434$ s . Thus, the maximum RTA at the vertiport is RTA = 531 s .

图 7 展示了根据第 III.C 节中的电池模型，执行图 6 中每条轨迹所需的 SOC。我们假设电池容量为 $Q = 5000$ Ahr 和标称电压 $V_n = 12$ V 。例如，图 7 显示，对于剩余的 SOC = 25% ，在进近定位点的最新 RTA 是 $\text{RTA}_{af} = 434$ s 。因此，在垂直机场的最大 RTA 是 RTA = 531 s 。

B. Rolling-Horizon Arrival Sequencing and Scheduling for a 1-Day eVTOL Arrival Demand

B. 针对一日 eVTOL 到达需求的滚动窗口到达排序与调度

In this section we present the results of the rolling-horizon EHANG 184 arrival sequencing and scheduling optimization model. We run the optimization algorithm at the current time within a certain look-ahead planning period such as 5 and 10 min (see Table 1). After we calculate the RTAs for the flights in the current planning horizon, we fix the RTAs and sequencing obtained up to this moment and move to next planning horizon. Next, we consider the new eVTOL arrivals, and run the optimization algorithm again. We assume 1 day of operations demand, as introduced in Sec. III.E.

在本节中，我们展示了滚动窗口 EHANG 184 到达排序与调度优化模型的结果。我们在当前时间内在一定的前瞻规划期内运行优化算法，例如 5 和 10 min (见表 1)。计算完当前规划期内航班的 RTAs 后，我们固定至此时刻获得的 RTAs 和排序，并移动到下一个规划窗口。接下来，我们考虑新的 eVTOL 到达，并再次运行优化算法。我们假设一天的操作需求，如第 III.E 节中所述。

Table 1 Computational time for the rolling-horizon eVTOL arrival sequencing and scheduling problem

表 1 滚动窗口 eVTOL 到达排序与调度问题的计算时间

Length planning period, min	5	10	15	20
Average computational time per planning horizon, s	5.7	76	190	510

规划期长度，分钟	5	10	15	20
每个规划时段的平均计算时间，秒	5.7	76	190	510

For the eVTOL arrival sequencing and scheduling optimization model, we consider $c_e^p = 0, c_l^p = 28, c_{l.af}^p = 36$, and $c_{l.h}^p = 42$, where $c_l^p = 28$ is the energy differential of a shallow descent trajectory that requires one additional second to be flown, that is, $(\Delta E/\Delta t) = 28$ kW; $c_{l,af}^p = 36$ is the power required to fly at cruise altitude and velocity; and $c_{l,h}^p = 42$ is the power required to hover. Lastly, $c_e^p = 0$ since, for EHANG 184, the most energy-efficient trajectory, after using GPOPS-II, also corresponds to the earliest possible arrival time at the approach fix, that is, $\text{RTA}_{af} = 165$ s . We also assume $K = 2$ [27].

对于 eVTOL 到达顺序和调度优化模型，我们考虑 $c_e^p = 0, c_l^p = 28, c_{l.af}^p = 36$ 和 $c_{l.h}^p = 42$ ，其中 $c_l^p = 28$ 是浅降轨迹所需的额外一秒钟飞行的能量差，即 $(\Delta E/\Delta t) = 28$ kW; $c_{l,af}^p = 36$ 是在巡航高度和速度下飞行的所需功率；$c_{l,h}^p = 42$ 是悬停所需的功率。最后，$c_e^p = 0$ 由于对于 EHANG 184，使用 GPOPS-II 后最节能的轨迹也对应于在进近定位点最早可能的到达时间，即 $\text{RTA}_{af} = 165$ s 。我们还假设 $K = 2$ [27]。

Figure 8 shows eVTOL arrivals over 1 day of operations, which are generated based on the demand model [8] in Sec. III.E.

图 8 显示了在一天运营时间内 eVTOL 的到达情况，这些是基于第 III.E 节中需求模型 [8] 生成的。

We compared our arrival sequencing and scheduling algorithm with a baseline heuristic algorithm called first-come-first-serve (FCFS). In Figs. 9 and 10 , we can observe that our algorithm dominates the FCFS through a 24 h period in both reducing average delay and maximum delay. In air traffic control, the FCFS algorithm is a commonly used heuristic to mimic human controller's tactical decision-making process. Specifically, in this application, the FCFS logic tries to first schedule the eVTOL aircraft to the minimum ETA between the ETA to fix A and the ETA to fix B. If this minimum ETA is the ETA to fix A and fix A is available (satisfying time separation constraint), then we schedule the eVTOL to fix A. If the minimum ETA is the ETA to fix B and fix B is available, then we schedule it to fix B. If the minimum ETA is the ETA to fix A and fix A is not available, but fix B is available, then we schedule it to fix B. If the minimum ETA is the ETA to fix B and fix B is not available, but fix A is available, then we schedule it to fix A. In all cases, if the RTA exceeds the RTA upper bound according to the SOC, then we do not schedule this eVTOL. This corresponds to the case when, for instance, the eVTOL is redirected to another landing pad.

我们将我们的到达顺序和调度算法与一个基线启发式算法——先来先服务 (FCFS) 进行了比较。在图 9 和 10 中，我们可以观察到，我们的算法在减少平均延迟和最大延迟方面均优于 FCFS 算法，持续时间 24 h 。在空中交通管制中，FCFS 算法是一种常用的启发式方法，用于模拟人类管制员的战术决策过程。具体来说，在这个应用中，FCFS 逻辑首先尝试将 eVTOL 飞机调度到 ETA to fix A 和 ETA to fix B 之间的最小 ETA。如果这个最小 ETA 是 ETA to fix A，并且 fix A 可用 (满足时间分离约束)，那么我们将 eVTOL 调度到 fix A。如果最小 ETA 是 ETA to fix B，并且 fix B 可用，那么我们将它调度到 fix B。如果最小 ETA 是 ETA to fix A，fix A 不可用，但 fix B 可用，那么我们将它调度到 fix B。如果最小 ETA 是 ETA to fix B，fix B 不可用，但 fix A 可用，那么我们将它调度到 fix A。在所有情况下，如果 RTA 超过了根据 SOC 确定的 RTA 上限，那么我们不会调度这个 eVTOL。这对应于例如 eVTOL 被重定向到另一个着陆垫的情况。

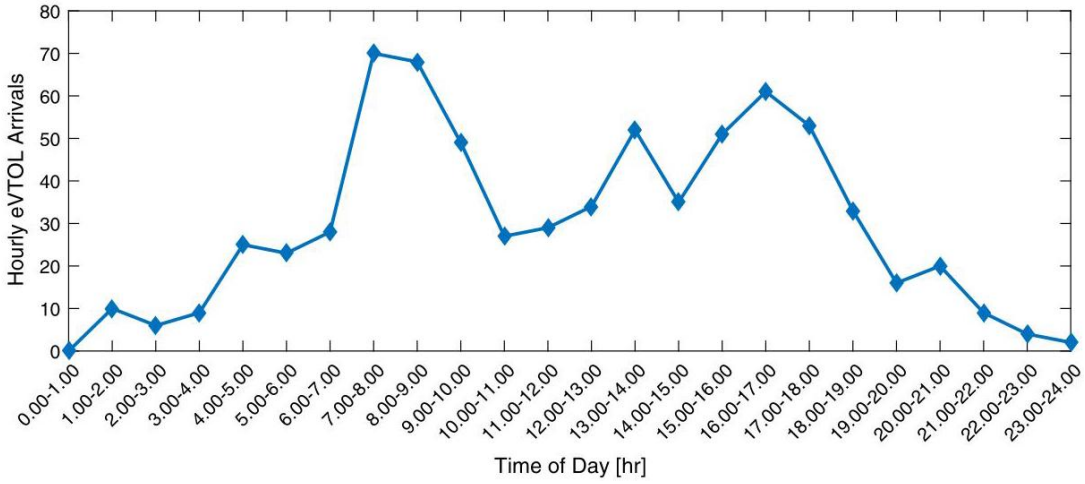

Fig. 8 Hourly eVTOL arrivals at the hub vertiport.
图 8. 每小时 eVTOL 在中心直升机场的到达情况。

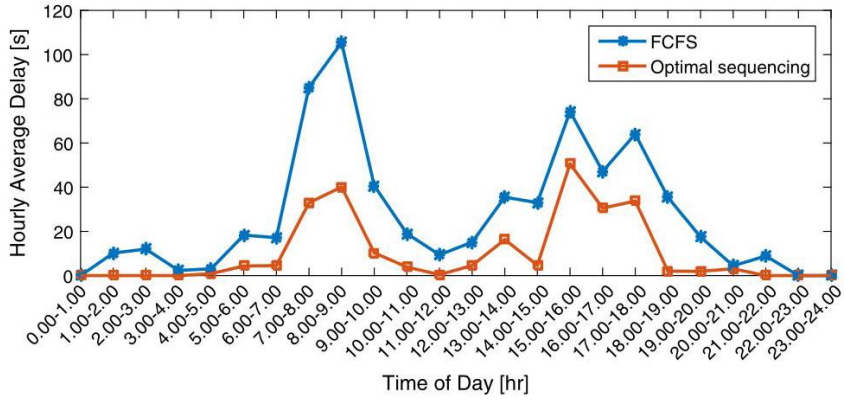

Fig. 9 Average eVTOL delay at the vertiport for 1 day.
图 9. 1 天内直升机场的平均 eVTOL 延迟。

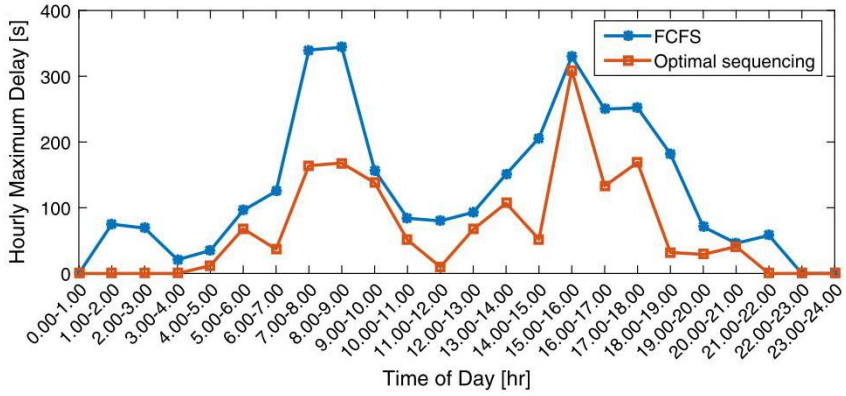

Fig. 10 Hourly maximum eVTOL delay at a double-landing-pad vertiport.
图 10. 双着陆垫直升机场每小时最大 eVTOL 延迟。

Figure 9 shows the average delay, that is, (RTA - ETA), imposed on eVTOLs arriving at the vertiport. Let us focus on discussing the result of our scheduling algorithm (the orange curve). In accordance to the demand peaks in Fig. 8, the eVTOLs start to experience delays from early morning at $\overline{7}$: 00 a.m. until 9:00 a.m., with the highest average delay of 40 s . The eVTOL delays decrease significantly after

10:00 a.m. From 3:00 p.m., eVTOLs start experiencing higher delays again, with a highest average delay of 50 s . Figure 10 shows the maximum amount of delay that eVTOLs experience when arriving at the vertiport. Again, the highest delays occur around the peak demand hours, between 8:00 a.m. and 9:00 a.m. (168 s) and between 3:00 p.m. and 4:00 p.m. (309 s).

图 9 显示了到达立体港口的 eVTOLs 所承受的平均延迟，即 (RTA - ETA)。让我们集中讨论我们的调度算法结果 (橙色曲线)。根据图 8 的需求高峰，eVTOLs 从早上 $\overline{7}:00$ 开始经历延迟，直到上午 9:00，最大平均延迟为 40 s 。上午 10:00 之后，eVTOLs 的延迟显著减少。从下午 3:00 开始，eVTOLs 再次开始经历更高的延迟，最大平均延迟为 50 s 。图 10 显示了 eVTOLs 到达立体港口时经历的最大延迟。同样，最大延迟出现在需求高峰时段，即早上 8:00 到 9:00(168 秒) 和下午 3:00 到 4:00(309 秒)。

Table 1 shows both the computational time required to sequence and schedule, using a rolling-horizon approach, 1 day of operations, as well at the computational time for one planning horizon only. The results are obtained using CPLEX LP Solver extension of MATLAB on a computer with Intel CORE i7 processor. Table 1 shows that the required computational time is significantly high for a planning horizon of 15 min or more. The use of short planning periods is, however, suitable for on-demand UAM, where demand for eVTOLs occurs ad-hoc during the day.

表 1 显示了使用滚动窗口方法对一天的操作进行排序和调度所需的计算时间，以及仅对一个规划时段的计算时间。这些结果是在配备 Intel CORE i7 处理器的计算机上使用 MATLAB 的 CPLEX LP 求解器扩展获得的。表 1 显示，对于 15 min 或更多的规划时段，所需的计算时间显著增加。然而，使用较短的规划时段适合按需 UAM，因为在一天中，对 eVTOL 的需求是临时发生的。

Figure 11 shows the impact of the minimum time separation between consecutive arrivals at the vertiport on the delay experienced by the eVTOLs. Increasing the time separation from 90 to 100 s shows that, during peak demand hours around 8:00 a.m. and 4:00 p.m., the eVTOL delays increase by up to 75% . In contrast, a time separation of 60 s results in eVTOL delay of at most 10 s , even during peak demand hours. Thus, designing eVTOLs for low time separation requirements is beneficial for on-time operations.

图 11 显示了连续到达机场的最低时间间隔对 eVTOL 经历的延误影响。将时间间隔从 90 增加到 100 s 显示，在上午 8:00 和下午 4:00 的峰值需求时段，eVTOL 的延误增加了高达 75% 。相比之下，60 s 的时间间隔使得即使在峰值需求时段，eVTOL 的延误最多也只有 10 s 。因此，为低时间间隔要求设计 eVTOL 有利于按时运行。

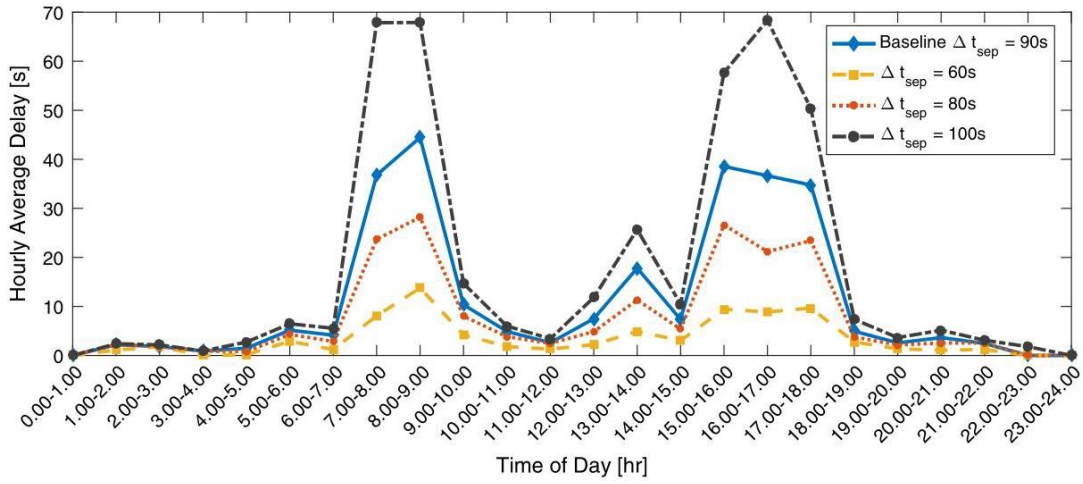

Fig. 11 Average eVTOL delay at a double-landing-pad vertiport-various minimum time separations.
图 11 双降落垫机场的平均 eVTOL 延误 - 不同的最低时间间隔。

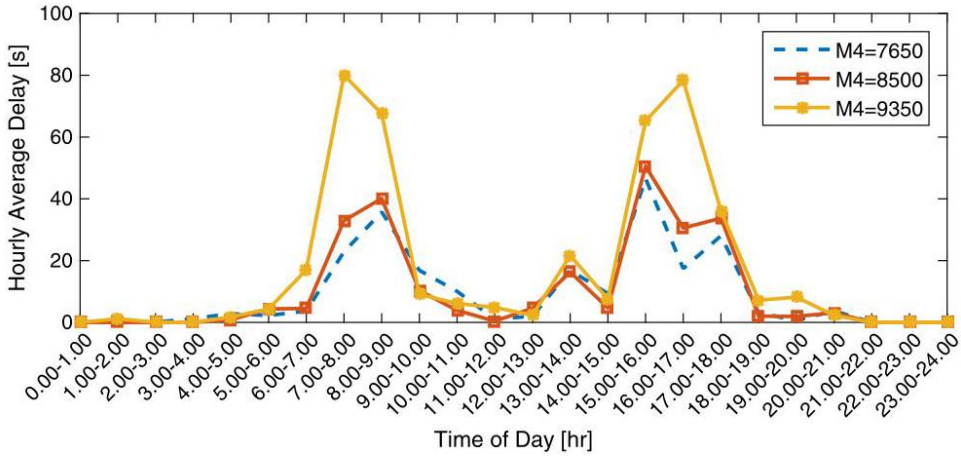

Fig. 12 Average eVTOL delay at a double-landing-pad vertiport-various coefficients of the eVTOL demand model.

图 12 双降落垫机场的平均 eVTOL 延误 - 不同的 eVTOL 需求模型系数。

In Fig. 12, the performance of the scheduling model in terms of hourly expected delays is shown for different scaling coefficient M_4 of the eVTOL demand (see Sec. III.E). The results show that, for an increase of 10% in the scaling coefficient, that is, $M_4 = 9350$, the expected delay during peak hours is almost double, compared with the baseline demand model with $M_4 = 8500$. The impact on delay is less for a decrease of 10% in the scaling coefficient, that is, $M_4 = 7650$.

在图 12 中，展示了不同缩放系数 M_4 的 eVTOL 需求 (参见第 III.E 节) 下，调度模型在每小时预期延误方面的性能。结果显示，当缩放系数增加 10% ，即 $M_4 = 9350$ 时，峰值时段的预期延误几乎是基准需求模型 $M_4 = 8500$ 的两倍。而当缩放系数减少 10% ，即 $M_4 = 7650$ 时，对延误的影响较小。

C. Monte Carlo Simulation of eVTOL Operations Demand

C. eVTOL 运行需求的蒙特卡洛模拟

We perform a Monte Carlo simulation of the demand of eVTOL operations (see Sec. III.E [8]) and evaluate the distribution of eVTOL delays. In particular, we consider that eVTOLs arrive at an area of radius 3900 m around the vertiport according to a stochastic process. Also, the initial SOC of the batteries is assumed to follow a Gaussian distribution. For computational purposes, we evaluate two demand periods only: 1) a peak demand period between 7:30 a.m. to 8:30 a.m. and 2) an off-peak demand period during noon time, from 11:30 a.m. to 12:30 p.m., when half as many eVTOL arrivals as in the peak period are expected to occur (see Fig. 4).

我们对电子垂直起降飞行器 (eVTOL) 运营需求进行了蒙特卡洛模拟 (见第 III.E 节 [8])，并评估了 eVTOL 的延误分布。特别是，我们考虑 eVTOL 根据随机过程到达半径为 3900 m 的机场周边区域。此外，假设电池的初始荷电状态 (SOC) 遵循高斯分布。出于计算目的，我们仅评估两个需求时段:1) 高峰需求时段，即上午 7:30 至 8:30；2) 非高峰需求时段，即中午时分，从上午 11:30 至下午 12:30，预计到达的 eVTOL 数量将是高峰时段的一半 (见图 4)。

Figures 13 and 14 show that in off-peak periods, up to 94% of the arriving eVTOLs experience at most 1 min delay. However, in the peak period, only 72% of the arriving eVTOLs experience at most 1 min delay, with 24% of the eVTOLs having a delay of $1 - 3$ min .

图 13 和图 14 显示，在非高峰时段，多达 94% 的到达 eVTOLs 最多经历 1 min 的延误。然而，在高峰时段，只有 72% 的到达 eVTOLs 最多经历 1 min 的延误，其中 24% 的 eVTOLs 有 $1 - 3$ min 的延误。

Figure 15 shows the distribution on the eVTOL arrival delays when considering a single- and a double-landing-pad vertiport, respectively. The eVTOL arrival sequencing and scheduling optimization model for a vertiport with one landing pad has been considered in [15]. The model in [15] has been further extended by considering a rolling-horizon approach to determine an optimal eVTOL arrival schedule. Moreover, the model has been extended with the possibility for eVTOLs to hover at a distance $R + r$ from the vertiport.

图 15 显示了在考虑单降落垫和双降落垫机场的情况下，eVTOL 到达延误的分布。已经考虑了具有一个降落垫的机场的 eVTOL 到达顺序和调度优化模型 [15]。[15] 中的模型通过考虑滚动时间窗口方法来确

定最优 eVTOL 到达时间表进行了扩展。此外，模型还扩展了 eVTOL 在距离机场 $R + r$ 的地方悬停的可能性。

Figures 14 and 15 show that, during off-peak periods, having a double-landing-pad vertiport results in 94% of the arriving eVTOLs having at most 1 min delay. However, having a single-landing-pad vertiport results only in 56% of the arrivals experiencing at most 1 min delay, with 31% of the arrivals having a delay of $1 - 4$ min . We note that for the peak hour 7:30 a.m. to 8:30 a.m., due to the high number of eVTOL arrivals, a single landing pad cannot accommodate the demand; thus we have not considered this case for simulation.

图 14 和图 15 显示，在非高峰时段，拥有双降落垫的垂直机场会导致 94% 的抵达 eVTOLs 最多有 1 min 的延迟。然而，拥有单降落垫的垂直机场仅导致 56% 的抵达经历最多 1 分钟的延迟，其中 31% 的抵达有 $1 - 4$ min 的延迟。我们注意到在高峰时段 7:30 a.m. 至 8:30 a.m.，由于 eVTOL 抵达数量众多，单个着陆垫无法满足需求；因此我们在模拟中未考虑这种情况。

V. Discussion

V. 讨论

This paper addresses the eVTOL arrival sequencing and scheduling at a vertiport terminal airspace such that the arrival delays are minimized. We consider potential shallow descent approaches to induce arrival delay. In turn, we generate RTA for the incoming aircraft to enforce such delays. We envision that this arrival management model will complement predeparture planning/scheduling models and strategic air traffic flow management models, while supporting safe and efficient UAM operations.

本文解决了在垂直机场终端空域的 eVTOL 抵达顺序和调度问题，以最小化抵达延迟。我们考虑了可能产生的浅降方法以诱导抵达延迟。相应地，我们为 incoming aircraft 生成 RTA 以执行这些延迟。我们设想这种抵达管理模型将补充预先出发的计划/调度模型和战略空中交通流量管理模型，同时支持安全和高效的 UAM 运行。

In practice, we expect additional challenges for the eVTOL arrival process. First, the arrival process is impacted by the capacity of the vertiport and, in particular, by the eVTOL turnaround requirement. Although we consider arrival management to be one of the main priorities for UAM operations, due to eVTOL battery constraints and envisioned high traffic densities in the terminal area, it remains a challenge to analyze together the arrival, turnaround, and departure processes at a vertiport.

在实际操作中，我们预计 eVTOL 抵达过程会面临更多挑战。首先，抵达过程受到垂直机场容量影响，特别是受到 eVTOL 周转要求的影响。尽管我们将抵达管理视为 UAM 运营的主要优先事项之一，但由于 eVTOL 电池限制和预计的终端区域高交通密度，分析垂直机场的抵达、周转和出发过程仍然是一个挑战。

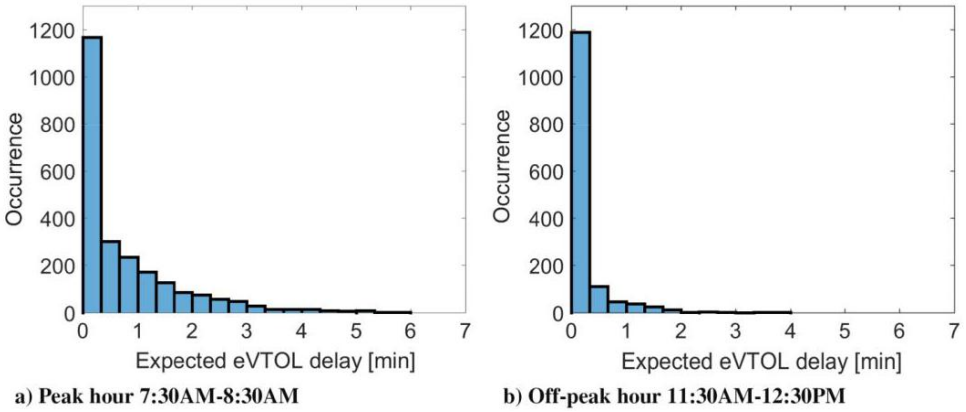

Fig. 13 Distribution of eVTOL delay for eVTOLs arriving at a double-landing-pad vertiport.
图 13 双降落垫垂直机场抵达 eVTOL 的延迟分布。

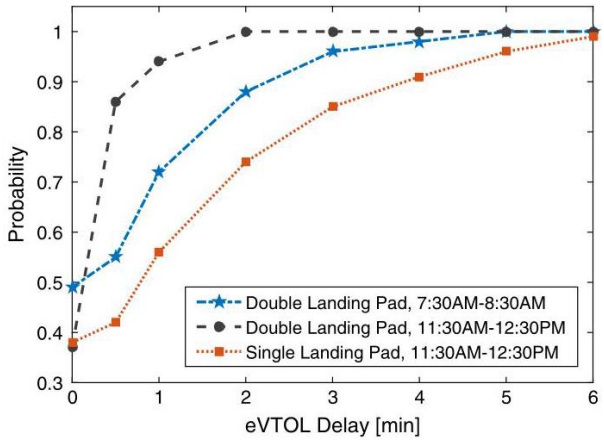

Fig. 14 Cumulative distribution function for eVTOL delay.

图 14 eVTOL 延迟的累积分布函数。

Second, further analysis of the potential demand for eVTOL operations throughout a day is needed to assess arrival scheduling algorithms. In particular, dedicated arrival heuristics should be developed to account for extreme demand values. For instance, in our paper we analyzed the FCFS heuristic, which is commonly used for arrival sequencing and scheduling of commercial aviation. Lastly, the design of contingency plans, such as, for instance, eVTOL vectoring or hovering, should be investigated together with arrival management algorithms.

其次，需要对一天内 eVTOL 运营的潜在需求进行进一步分析，以评估到达调度算法。特别是，应开发专用的到达启发式方法来考虑极端需求值。例如，在我们的论文中，我们分析了 FCFS 启发式方法，这是常用于商业航空到达排序和调度的方法。最后，还应研究应急计划的设计，例如 eVTOL 的矢量引导或悬停，以及与到达管理算法的结合。

VI. Conclusions

VI. 结论

In this paper, a double-landing-pad vertiport where on-demand eVTOLs arrive is considered. An optimal, rolling-horizon eVTOL sequencing and scheduling algorithm is proposed such that time deviations from a preferred arrival time are minimized. The optimization problem is formulated as a mixed-integer linear program with constraints regarding the minimum time separation, electrical battery discharge, and vehicle dynamics. The discharge battery model, in particular, makes this arrival scheduling algorithm specially designed for eVTOL operations. The sequencing and scheduling problem is solved using a rolling-horizon approach for 1 day of operations, where the demand for operations corresponds to a hexagonal verti-port network in Houston, TX. Our proposed sequencing and scheduling algorithm has arrival route selection capability. The algorithm outputs landing time slots (or RTAs) for all arriving eVTOLs to achieve minimum total delay. The distribution of delays imposed on the arriving eVTOLs at the vertiport is determined. It is shown that a double-landing-pad vertiport is able to accommodate the demand in both off-peak and peak hours, with eVTOLs average delays up to 50 s in peak hours.

本文考虑了一个双降落垫的垂直机场，在这里按需到达的 eVTOLs。提出了一种最优的、滚动时间段的 eVTOL 排序和调度算法，以最小化与预定到达时间的偏差。优化问题被表述为一个混合整数线性规划，其约束条件包括最小时间间隔、电池放电和车辆动力学。特别是，放电电池模型使得这个为 eVTOL 运营特别设计的到达调度算法。排序和调度问题通过滚动时间段方法解决，适用于 1 天的运营，其中运营需求对应于德克萨斯州休斯顿的六边形垂直机场网络。我们提出的排序和调度算法具有到达路线选择能力。算法为所有到达的 eVTOLs 输出着陆时间槽 (或 RTAs)，以实现最小总延迟。确定了在垂直机场对到达的 eVTOLs 施加的延迟分布。结果表明，双降落垫的垂直机场能够在非高峰和高峰时段满足需求，eVTOLs 在高峰时段的平均延迟达到 50 s 。

Future work will include 1) exploring other heuristics to achieve near-real-time, suboptimal solutions under high eVTOL demands; 2) design of terminal airspace and estimation of vertiport capacities; 3) accounting for uncertainties with respect to the eVTOL flight performance; and 4) investigating other delay absorption concepts such as ground delay at the departure vertiport, hovering, and vectoring.

后续工作将包括 1) 探索其他启发式方法，以在高 eVTOL 需求下实现接近实时、次优解决方案；2) 设计终端空域和估算垂直机场容量；3) 考虑与 eVTOL 飞行性能相关的确定性；以及 4) 调查其他延迟吸收概念，例如起飞垂直机场的地面延迟、悬停和向量控制。

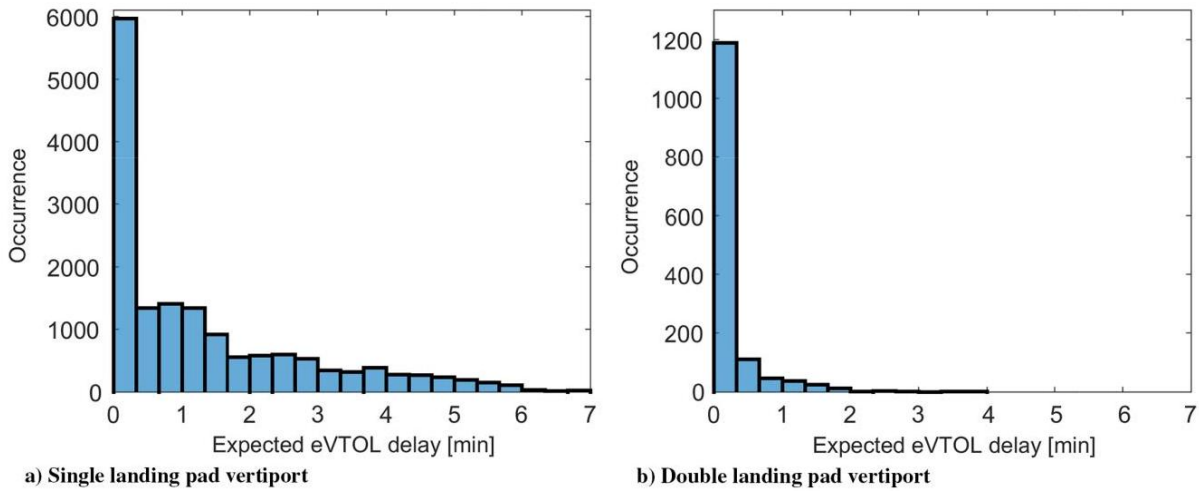

Fig. 15 Distribution of eVTOL delay during an off-peak hour 11:30 a.m. to 12.30 p.m.
图 15 呈现了非高峰时段 (上午 11:30 至下午 12:30)eVTOL 延迟的分布情况。

References

参考文献

[1] Polaczyk, N., Trombino, E., Wei, P., and Mitici, M., "A Review of Current Technology and Research in Urban On-Demand Air Mobility Applications," 8th Biennial Autonomous VTOL Technical Meeting and 6th Annual Electric VTOL Symposium, Mesa, Arizona, 2019.

[2] "Fast-Forwarding to a Future of On-Demand Urban Air Transportation," Uber Elevate Tech. Rept., Uber Elevate Whitepaper, 2016, uber.com/ elevate/whitepaper [accessed 10 Dec. 2019].

[3] Guérert, C., Prins, C., and Sevaux, M., Applications of Optimization with XPress-MP, Dash Optimization, Eyrolles, Paris, 2000, pp. 82-103, Chap. 7.

[4] Pawelek, A., Lichota, P., Dalmau, R., and Prats, X., "Arrival Traffic Synchronisation with Required Time of Arrivals for Fuel-Efficient Trajectory," Proceedings of the 17th ATIO-AIAA Aviation Technology, Integration, and Operations Conference, 2017, pp. 1-14.

[5] Hu, X., and Chen, W., "Genetic Algorithm Based on Receding Horizon Control for Arrival Sequencing and Scheduling," Engineering Applications of Artificial Intelligence, Vol. 18, No. 5, 2005, pp. 633-642. https://doi.org/10.1016/j.engappai.2004.11.012

[6] Vascik, P., and Hansman, J., "Constraint Identification in On-Demand Mobility for Aviation Through an Exploratory Case Study of Los Angeles," Proceedings of 17th AIAA Aviation Technology, Integration, and Operations Conference, 2017, pp. 1-25.

[7] Alonso, J., Arneson, H., Melton, J., Vegh, M., Walker, C., and Young, L., "System-of-Systems Considerations in the Notional Development of a Metropolitan Aerial Transportation System," Tech. Rept., Stanford Univ. and NASA Ames Research Center, 2017, https://nari.arc.nasa .gov/sites/default/files/Young_HopperII_N [accessed 10 Dec. 2019].

[8] Kohlman, L., and Patterson, M., "System-Level Urban Air Mobility Transportation Modeling and Determination of Energy-Related Constraints," Proceedings of Aviation Technology, Integration, and Operations Conference, AIAA Paper 2018-3677, 2018.

[9] Olive, X., and Morio, J., "Trajectory Clustering of Air Traffic Flows Around Airports," Aerospace Science and Technology, Vol. 84, Jan. 2019, pp. 776-781.
https://doi.org/10.1016/j.ast.2018.11.031

[10] Bennell, J. A., Mesgarpour, M., and Potts, C. N., "Airport Runway Scheduling," 40R-A Quarterly Journal of Operations Research, Vol. 9, No. 2, 2011, p. 115-138.
https://doi.org/10.1007/s10288-011-0172-x

[11] Ozgur, M., and Cavcar, A., "0-1 Integer Programming Model for Procedural Separation of Aircraft by Ground Holding in ATFM," Aerospace Science and Technology, Vol. 33, No. 1, 2014, pp. 1-8. https://doi.org/10.1016/j.ast.2013.12.009

[12] Andreeva-Mori, A., Suzuki, S., and Itoh, E., "Rule Derivation for Arrival Aircraft Sequencing," Aerospace Science and Technology, Vol. 30, No. 1, 2013, pp. 200-209.

https://doi.org/10.1016/j.ast.2013.08.004

[13] Wu, Y., Sun, L., and Qu, X., "A Sequencing Model for a Team of Aircraft Landing on the Carrier," Aerospace Science and Technology, Vol. 54,

July 2016, pp. 72-87.

2016 年 7 月，第 72-87 页。

https://doi.org/10.1016/j.ast.2016.04.007

[14] Bosson, C., and Lauderdale, T., "Simulation Evaluations of an Autonomous Urban Air Mobility Network Management and Separation Service," Proceedings of Aviation Technology, Integration, and Operations Conference, AIAA Paper 2018-3365, 2018.

[15] Kleinbekman, I., Mitici, M., and Wei, P., "eVTOL Arrival Sequencing and Scheduling for On-Demand Urban Air Mobility," 37th AIAA/IEEE Digital Avionics Systems Conference (DASC), IEEE, New York, 2018.

[16] Cuong Chi, G., Bole, B., Hogge, E., Vazquez, S., Daigle, M., Celaya, J., Weber, A., and Goebel, K., "Battery Charge Depletion Prediction on an Electric Aircraft," Proceedings of the Annual Conference of the Prognostics and Health Management Society, Vol. 4, 2013, pp. 1-11.

[17] Bole, B., Daigle, M., and Gorospe, G., "Online Prediction of Battery Proceedings of the European Conference on the Prognostics and Health

18] Alnaqeb, A., Li, Y., Lui, Y., Pradeep, P., Wallin, J., Hu, C., Hu, S., and Wei, P., "Online Prediction of Battery Discharge and Flight Mission Assessment for Electrical Rotorcraft," Proceedings of AIAA Aerospace Sciences Meeting, AIAA Paper 2018-2005, 2018.

[19] Plett, G., Equivalent-Circuit Methods, Battery Management Systems, Vol. II, Artech House, Norwood, MA, 2016, pp. 69-80, Chap. 3.

[20] Goodrich, K., and Barmore, B., "Exploratory Analysis of the Airspace Throughput and Sensitivities of an Urban Air Mobility System," Proceedings of Aviation Technology, Integration, and Operations Conference, AIAA Paper 2018-3364, 2018.

[21] Pradeep, P., and Wei, P., "Energy Efficient Arrival with RTA Constraint for Urban eVTOL Operations," Proceedings of AIAA Aerospace Sciences Meeting, AIAA Paper 2018-2008, 2018, pp. 1-13.

[22] Erzberger, H., and Itoh, E., "Design Principles and Algorithms for Air Traffic Arrival Scheduling," NASA TP-2014-218302, NASA Ames Research Center, CA, 2014.

[23] "EHANG184 Autonomous Aerial Vehicle Specs," EHANG184, 2018, http://www.ehang.com/ehang184/specs/ [retrieved March 2018].

[24] Johnson, W., Rotorcraft Aeromechanics, Cambridge Univ. Press, Cambridge, 2013, pp. 39-81, Chap. 3.

[25] Patterson, M., and Rao, A., "GPOPS-II: A MATLAB Software for Solving Multiple-Phase Optimal Control Problems Using hp-Adaptive Gaussian Quadrature Collocation Methods and Sparse Nonlinear Programming," ACM Transactions on Mathematical Software (TOMS), Vol. 41, No. 1, 2014, pp. 1-37.

[26] Samà, M., D'Ariano, A., and Pacciarelli, D., "Optimal Aircraft Traffic Flow Management at a Terminal Control Area During Disturbances," Procedia-Social and Behavioral Sciences, Vol. 54, No. 1, 2014, pp. 460-469.

[27] Rodriguez-Diaz, A., Adenso-Diaz, B., and Gonzalez-Torre, P., "Minimizing Deviation from Scheduled Times in a Single Mixed Operation Runway," Computer Operations Research, Vol. 78, Feb. 2017, pp. 193-202.

https://doi.org/10.1016/j.cor.2016.09.014

M. J. Kochenderfer

M. J. Kochenderfer

Associate Editor

副编辑